Supplement for: Nanopore sequencing of the phi X 174 genome

Andrew H. Laszlo[1], Ian M. Derrington[1], Brian C. Ross[1], Henry Brinkerhoff[1], Andrew Adey[2], Ian C. Nova[1], Jonathan M. Craig[1], Kyle W. Langford[1], Jenny Mae Samson[1], Riza Daza[2], Kenji Doering[1], Jay Shendure[2], Jens H. Gundlach[1,†]

[1]Department of Physics, University of Washington, Seattle, WA 98195, USA
[2]Department of Genome Sciences, University of Washington, Seattle, WA 98195, USA
[†]Corresponding author. E-mail: gundlach@uw.edu

Table of Contents:

Supplementary Figure 1: Data reduction flow chart

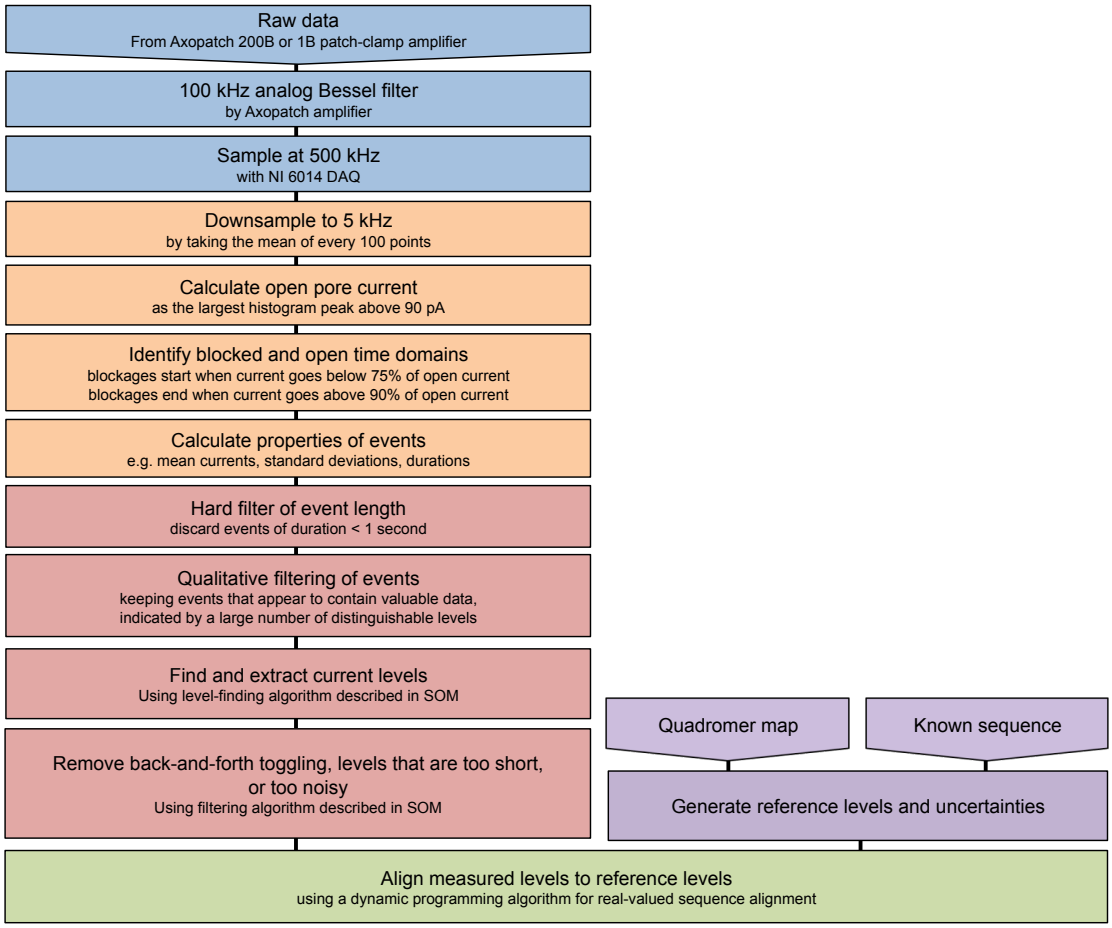

Supplementary Figure 2: Current consensuses for all de Bruijn strands 1-3

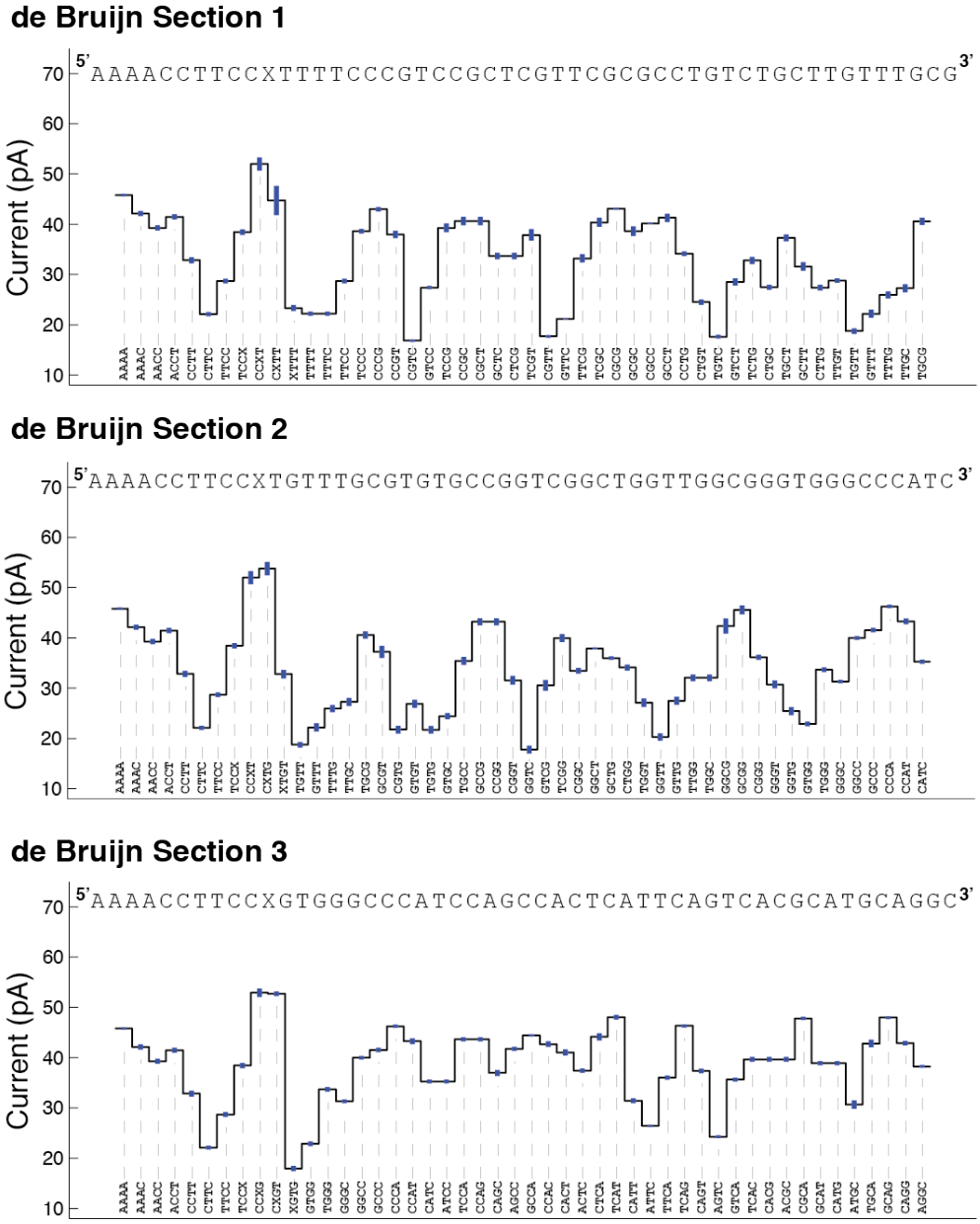

Supplementary figure 2: **de Bruijn sequence segments 1-3:** Consensus current level sequences and associated quadromers for de Bruijn segments 1-3. Consensuses for each strand were generated from 17, 11, and 15 reads of strands 1,2, and 3, respectively.

Supplementary Figure 3: Current consensuses for all de Bruijn strands 4-6

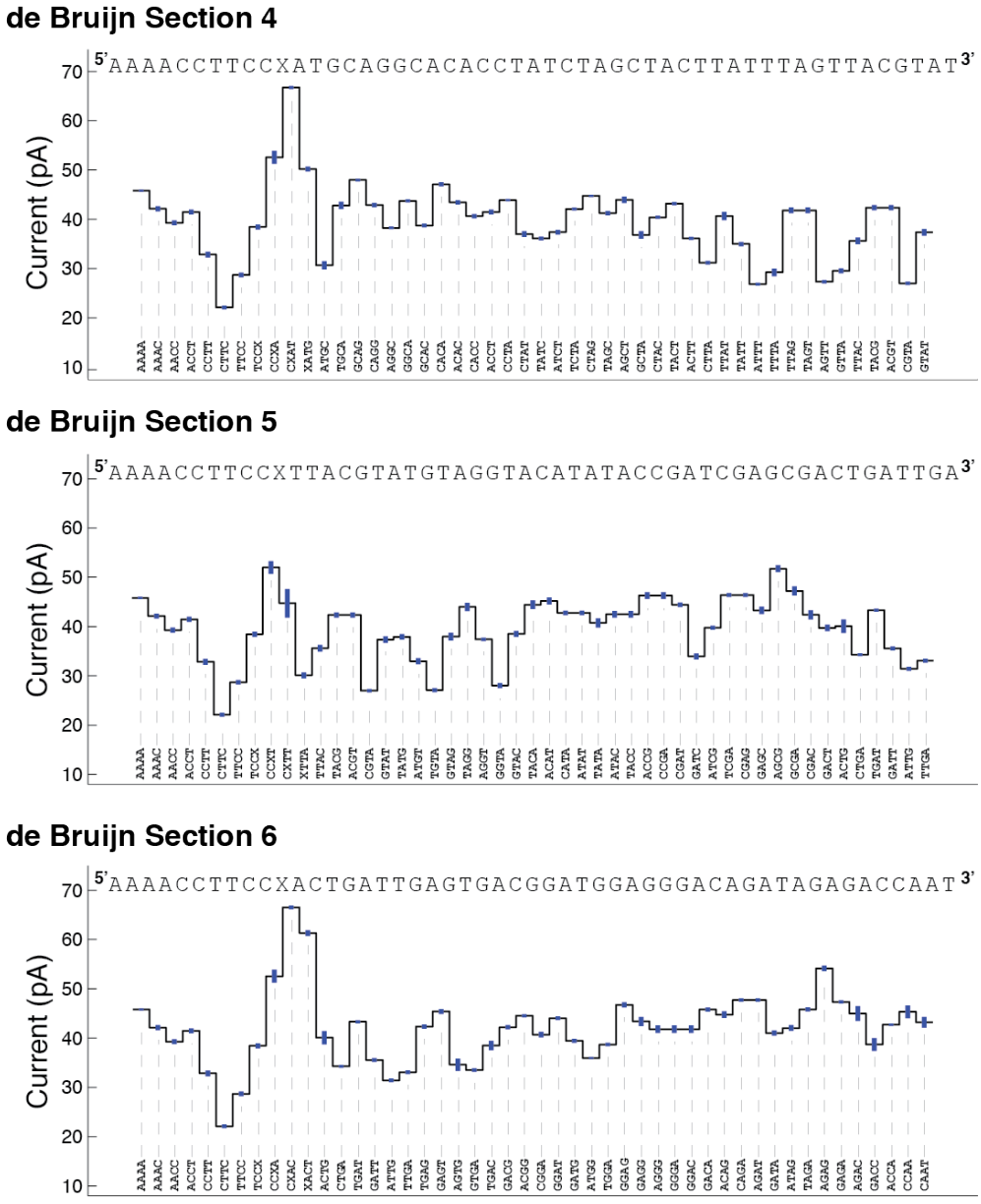

Supplementary figure 3: **de Bruijn segments 4-6:**Consensus current level sequences and associated quadromers for de Bruijn segments 4-6. Consensuses for each strand were generated from 12, 11, and 12 reads of strands 4,5, and 6, respectively.

Supplementary Figure 4: Current consensuses for all de Bruijn strands 7-8

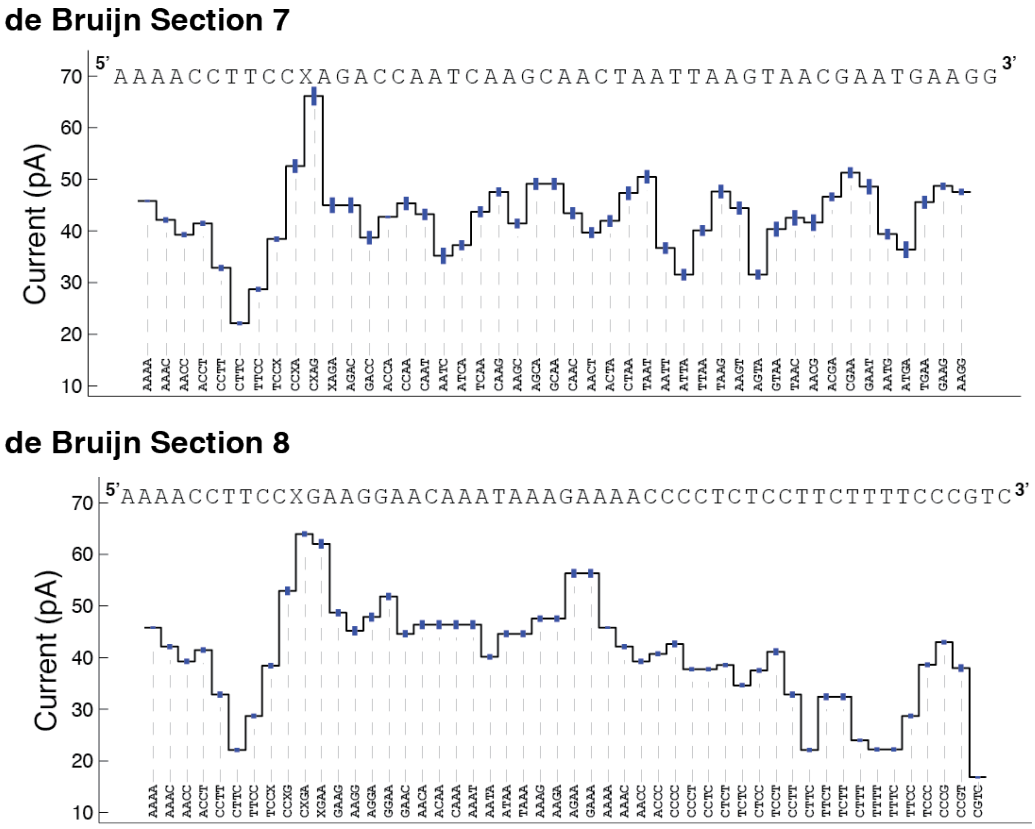

Supplementary figure 4: **de Bruijn segments 7-8.** Consensus current level sequences and associated quadromers for de Bruijn segments 7-8. Consensuses for each strand were generated from 14 and 7 reads of strands 7 and 8, respectively.

Description of automatic level finding algorithm

Our algorithm identifies levels in two steps. First, it identifies the level boundaries within the time-traces. Then it removes spurious levels and combines levels where the polymerase appears to have "toggled" between two bases.

Identifying level locations. Starting from the beginning of a current trace our technique first examines part of a current trace and divides it into two sections. Under the assumption that the sampled currents within each level are Gaussian-distributed, we compute the total probability that the two sections originated from two distinct Gaussian distributions. We divide this total probability by the probability of the null hypothesis, namely that the combination of the two sections originated from a single Gaussian. For ease of computation, we use log probabilities. For a given section the observed mean is $\hat{I}$ and width is σ. For an individual current measurement within this section, *I(t)*, at time *t*, the log probability (density) is:

$$\log p(I(t)) = \log\left(\frac{1}{\sqrt{2\pi}\sigma} e^{(I(t)-\hat{I})^2/2\sigma^2}\right) \qquad \text{Eq. 1.}$$

To find the total log probability that the observations between t_1 and t_2 belong to a single level defined by $\hat{I}$ and σ, we sum Eq. 1 between t_1 and t_2 and use the definition of sigma, giving

$$\log p(I([t_1, t_2])) = (t_2 - t_1)\log\sigma + \text{const} \qquad \text{Eq. 2.}$$

We calculate total log probability (Eq. 2) for each of the two sections between t_1 and t_2, and then between t_2 and t_3. To compare the log probabilities, we subtract the total log probability of the null hypothesis by computing Eq. 2 between t_1 and t_3. Combining all probabilities yields a comparison metric, which we denote log*p*(*t1,t2,t3*),

$$\begin{aligned}\log p(t_1, t_2, t_3) =& (t_2 - t_1)\log\sigma(t_2, t_1) + (t_3 - t_2)\log\sigma(t_3, t_2) \\ & - (t_3 - t_1)\log\sigma(t_3, t_1) + \text{const}\end{aligned} \qquad \text{Eq. 3.}$$

The t_2 yielding minimal log*p*(t_1, t_2, t_3) indicates the location of a possible level transition within the current observations between t_1 and t_3. In our level finding algorithm, we begin with a given time window ([t_1 ,t_3]) and search for t_2 that minimizes log*p*. If min(log*p*) is less than a specified threshold (we used a threshold of log*p* = -50) there is a level transition at t_2, and we recursively search between t_1 and t_2 and between t_2 and t_3 for other level transitions. If min(log*p*) is above the threshold for the original time window then there are no transitions within t_1 and t_3 and we consider a larger window by increasing the value of t_3.

Not all levels correspond to the single nucleotide forward motion of the phi29 DNAP. We remove levels that (1) have durations < 500μs, (2) have mean values outside of expected ranges (10-70 pA) or (3) have an error in the mean greater than 5 pA. Finally, using the logp calculated using Eq. 3 above, we identify regions of levels that are similar, and combine the levels in them.

Description of alignment algorithm

Our tool for aligning level sequences is based on the well-known Needleman-Wunsch and Smith-Waterman algorithms for sequence alignment (1, 2). A Needleman-Wunsch or Smith-Waterman alignment of two base sequences A and B allows for gaps in both sequences. Due to possible gaps the optimal alignment between the first n_A bases of A and the first n_B bases of B is one of the following: 1) the optimal alignment between the first n_{A-1} bases of A and all n_B bases of B plus a gap in A; 2) the optimal alignment between all n_A bases of A and the first n_{B-1} bases of B plus a gap in B; or 3) the optimal alignment between the first n_{A-1} bases of A and the first n_{B-1} bases of B plus a final matched base in both sequences. Longer optimal alignments are recursively calculated from shorter optimal sub-alignments, and the entries in the alignment table (**sup. fig. 5a**) are filled from top-left to bottom-right.

The main complication in our experiment is that our level sequences sometimes step backwards. If we used the Needleman-Wunsch scheme directly each entry in the alignment table would depend on both the entry to the left (due to forward steps) and the entry to the right (due to backsteps), which in turn would depend on the entry in question. To fix this problem, we require each step in the alignment to advance sequence A forward by one, as shown in **Supplementary figure 5b**. Our alignment is therefore the optimal mapping of *every* level in sequence A to its corresponding level in sequence B (or a null level if no good match exists). Note that our alignment trace passes over rather than through skipped levels in sequence B (**Sup. fig. 5c**).

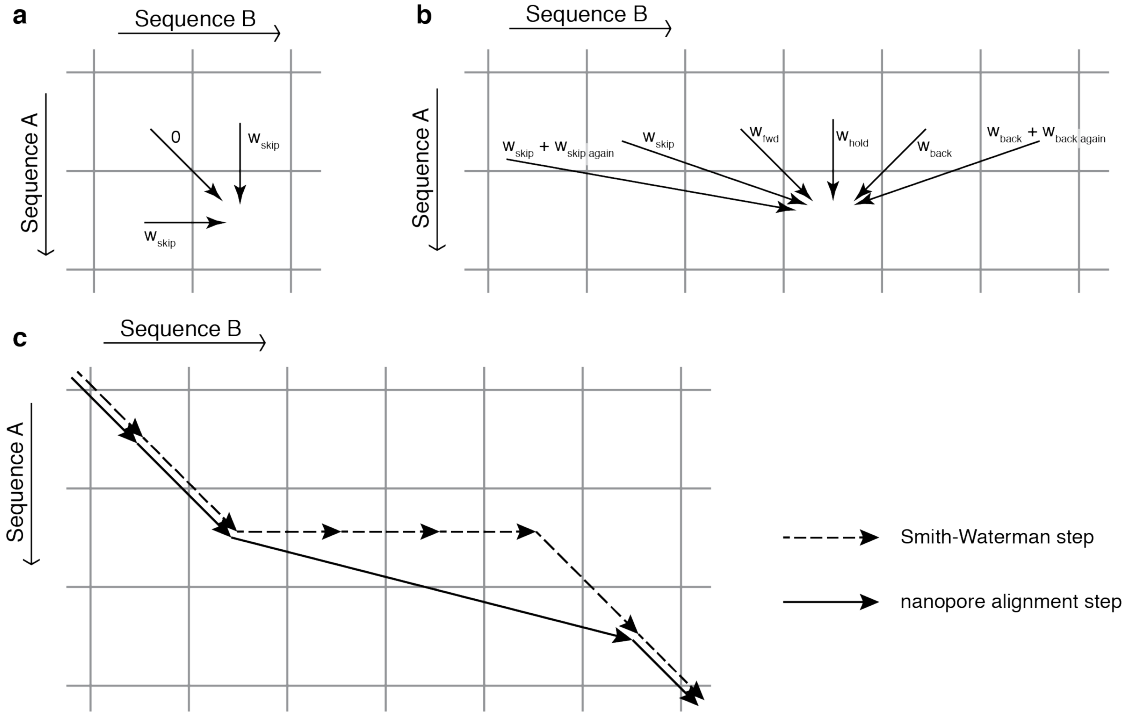

Supplementary figure 5: a) Needleman-Wunsch alignments consider horizontal and vertical steps in the alignment table (with a penalty w), corresponding to mismatched bases in one sequence or the other. Diagonal steps, indicating a matched base, generally have no penalty unless there is a mismatch. **b**) Our nanopore alignment forces every step to progress along sequence A, but allows backsteps in sequence B. We assign affine penalties to skips and backsteps: for example, a backstep of 3 levels would earn the backstep penalty w_{back} plus twice the backstep-again penalty $w_{backagain}$. **c**) The difference between a Needleman-Wunsch alignment and our nanopore alignment when there is a skip in sequence B.

Supplementary figure 6: Alignment of nanopore reads to quadromer prediction:

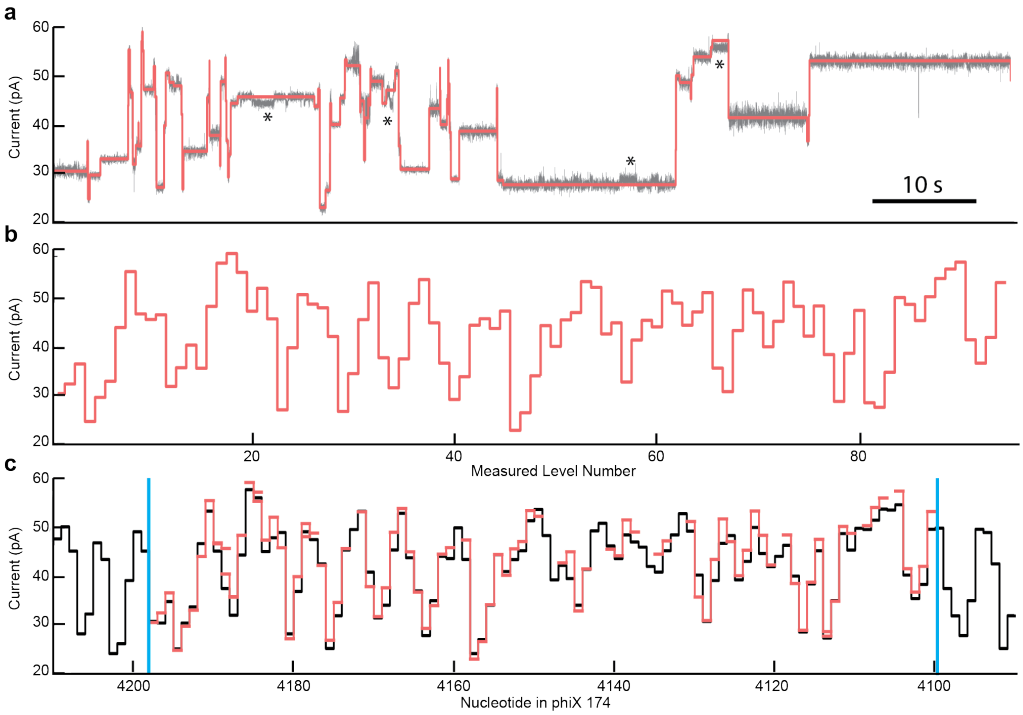

Supplementary figure 6. Similar to Fig. 3 in the main text, this figure demonstrates how alignment takes place. Instead of an amplicon being aligned, this figure shows a short sub-segment from a long event. **a**) Our level finding algorithm is used to identify transitions between levels in the current trace. Asterisks mark locations where the algorithm identifies and removes DNAP backsteps. **b**) We then extract the sequence of median current values from each level. **c**) Next, we align the current values to predicted values from the reference sequence using a dynamic programming alignment algorithm similar to Needleman-Wunch alignment (1). In some locations, levels are skipped in the nanopore read either due to motions of the DNAP or errors by the level finding algorithm. We determine read boundaries from the first and last matched levels in the reference sequence. Read boundaries are indicated by the blue lines.

Calculating alignment significance

Using the afore mentioned alignment algorithm we align nanopore reads to the predicted level sequence from a known DNA sequence using the quadromer map. The alignment produces a raw score, s, that can be compared to alignments to other reference sequences. Next, we generate a large random sequence along with the expected current levels. We then perform alignments of our measured data to the random sequence. If our measured levels are truly from phi X 174 we expect the score to stand out from the distribution of scores to random alignments. **Supplementary figure 7** shows a histogram of the scores for random alignments (blue) and a marker (red) for the location of the score for the alignment to phi X 174. Strongly negative scores represent good alignments.

Supplementary figure 7: The probability distribution of scores for random alignments dP/dS (blue), together with a marker (red) showing the location of the score of the alignment to phi X 174. Units are in arbs. This plot is made using event number 49 from figure 4 of the main

The confidence in the alignment C is calculated by

$$C(S_0) = \int_{-\infty}^{S_0} \frac{dP}{dS} dS$$

.

C represents the probability that a given alignment to a random sequence will produce a score better than S_0. This particular alignment had a confidence score of 10^{-147}, reflecting a high probability of these measured levels belonging to phi X 174 relative to random alignments. We assume that in the limit of an infinite number of random alignments, the distribution of alignment scores for random sequences approximate a Gaussian, so that

$$C(S_0) = \int_{-\infty}^{S_0} G(S) dS$$

.

We find the Gaussian by fitting to the width and center of the measured score distribution as floating parameters.

We comment briefly on the meaning of C because of the extreme smallness of these numbers. C represents nothing more than the probability that the produced alignment could also be randomly obtained. The score of 10^{-147} was produced by an alignment of nanopore read of length ~2000.

Supplementary figure 8: Coverage plot for phi X 174 amplicons

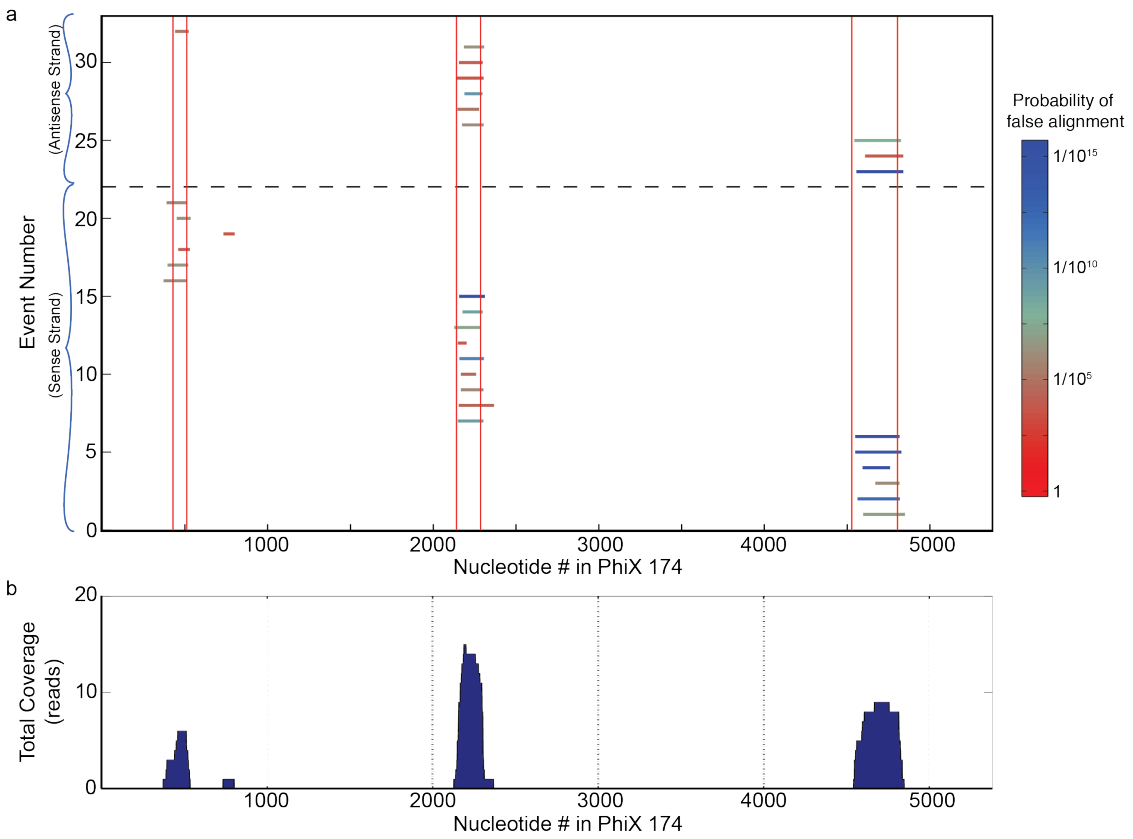

Supplementary figure 8: Amplicon alignment. 31 reads of phi X 174 amplicons aligned to current reference generated by translating the known phi X 174 sequence into current levels using the quadromer map. DNA strands are identified with high confidence, which enables a number of different useful applications such as organism identification and providing a reconstruction scaffold for short high-quality reads obtained with other sequencing technologies. **a**) Alignment bounds for 31 nanopore reads of phi X 174 amplicons. The alignment bounds match well with the actual amplicon locations. All reads with a quality better than 1 in 10^4 fall within one of three locations along the phi X 174 genome revealing the correct location of the amplicons within the genome. Because the adaptors attach to the strands in random orientation, we made reads of both the sense and anti-sense strands. **b**) Coverage for nanopore reads in **a**).

Supplementary figure 9: Full phi X 174 library gel

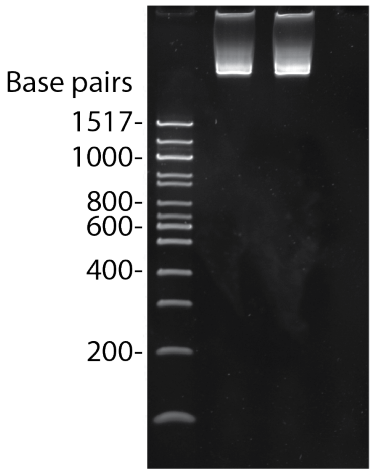

Supplementary figure 9: The gel shows the length distribution of phi X 174 genomic DNA used in our experiments (lanes 2 & 3 are replicates). There is a single band that contains broadening towards longer strand lengths. The band broadening is likely due to different numbers of ligated adaptors (0,1, or 2), different adaptor orientations (fan-tail or hairpin), or possibly circular forms of phi X 174. The absence of bands of shorter lengths indicates that our nanopore read lengths are determined not by library quality, but instead by how far the enzyme processes along the DNA before dissociating.

Phi X 174 consensus and quadromer map revision

We used values from a current level consensus for the phi X 174 genome to update the quadromer map. To generate the consensus current level sequence for phi X 174, we aligned each nanopore read of the phi X 174 DNA to the predicted current level sequences for its sense and antisense base sequences. The predicted current level sequences were made from the initial measurements of quadromers in the de Bruijn sequence. Alignments with an overall confidence better than 10^{-6} were selected to contribute to the updated map.

Only levels aligned with high certainty contributed to the consensus. All consensus level values were the average of at least four reads. Also, at least half of all reads covering this level contained a current level matched to that predicted level. The consensus value for the given context was calculated as the mean of all reads aligned to that level.

With the exception of the self complimentary quadromer GATC, there are many instances (35 on average, see **sup. fig. 10**) of each of the remaining 255 quadromers within the 5386-nucleotide phi X 174 genome and its complementary strand. For GATC, we retain the original de Bruijn sequence current value. Using the updated consensus levels, we were able to update the quadromer map with additional measurements in a variety of sequence contexts. The revised map uses the mean and standard deviation of all measurements made of each quadromer throughout the phi X 174 consensus (Table S2). **Supplementary figure 11** (next page) shows the revised quadromer map in comparison to the original quadromer map.

The consensus generation and quadromer map updating procedures were tested by reserving five high-quality reads to be excluded from the generation of the revised quadromer map, and then aligning these reads to both the consensus sequence and the updated prediction. In all cases, the confidence in the alignments of these reads improved dramatically when the new prediction was used as the reference sequence.

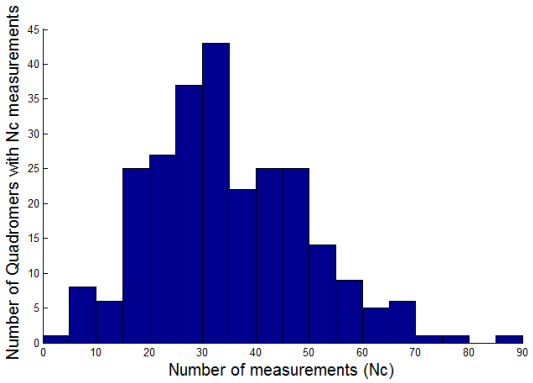

Supplementary figure 10: Histogram of the number of instances of each quadromer in the phi X genome. Each quadromer has 35 reads on average.

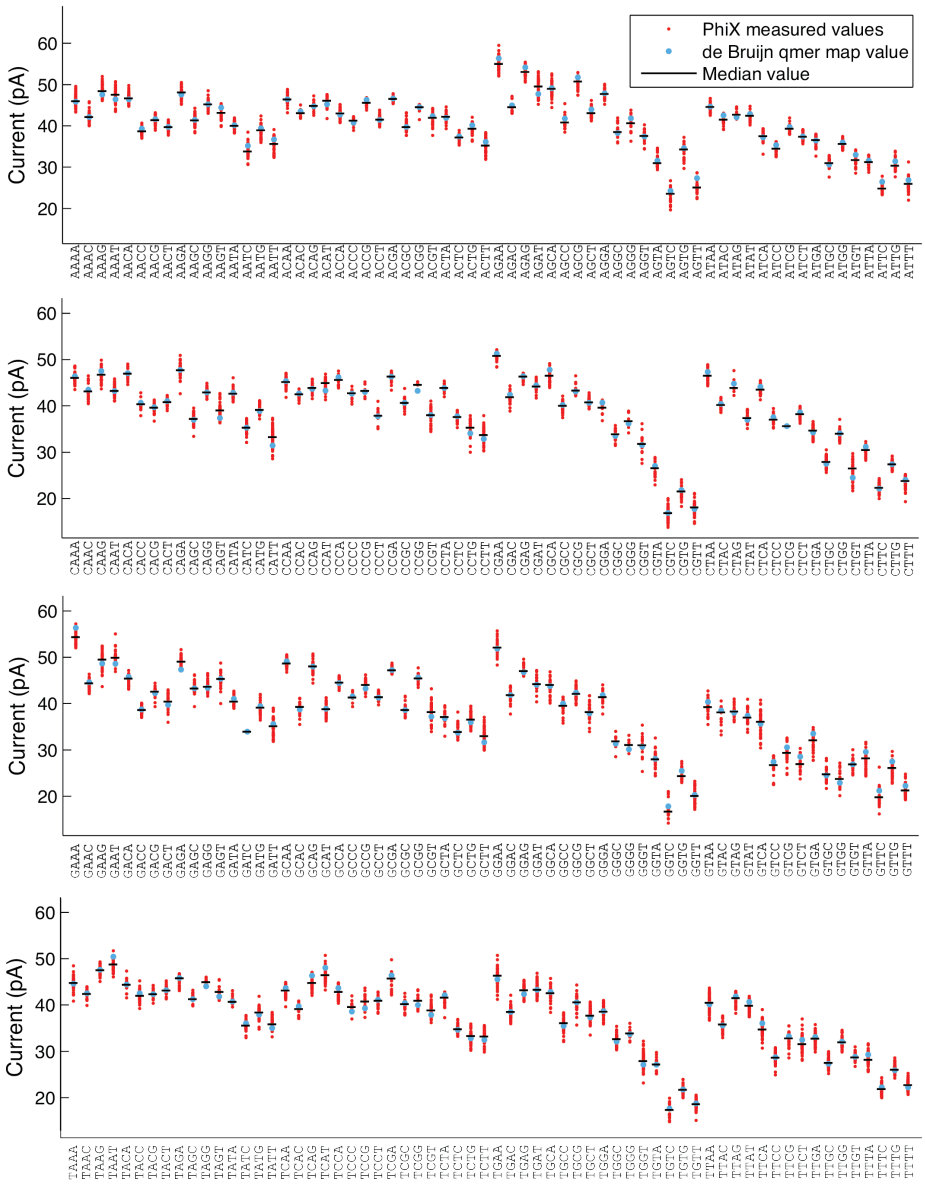

Supplementary figure 11: The revised quadromer map in alphabetical order, with 64 quadromers (written 5'-3') in each panel, beginning with A,C,G,T, respectively. Red dots are measured values of the quadromer in phi X 174. The blue dots are the values from the original de Bruijn quadromer map. The black lines are the medians of all measured instances of a given quadromer.

DNA scaffold reconstruction:

The difficulty of *de novo* sequencing with most sequencing technologies is that their many short DNA reads must be stitched together in the proper order to form a long contiguous sequence. This assembly process is usually performed by looking for sequence similarity between overlapping reads. We demonstrate an alternative method of sequence scaffolding by mapping 100 short, 100 bp long reads from an Illumina MiSeq sequencer to one of our long (3466 levels) nanopore read. The mapping was performed by converting the sequence of each Illumina read, and its reverse compliment, into a sequence of current levels using our quadromer map, and then using our level alignment tool to find the likely location of the current level sequence in our nanopore read. Figure S13 shows the fate of the 87 (out of 100) Illumina reads which generated an alignment to the nanopore read: 61 Illumina reads lay at least partially within the nanopore read and were aligned properly; 9 Illumina reads lay at least partially within the nanopore read and were misaligned; and 17 Illumina reads fell entirely outside the nanopore read. 9 of the 13 Illumina reads that did not generate an alignment actually lay outside the nanopore read.

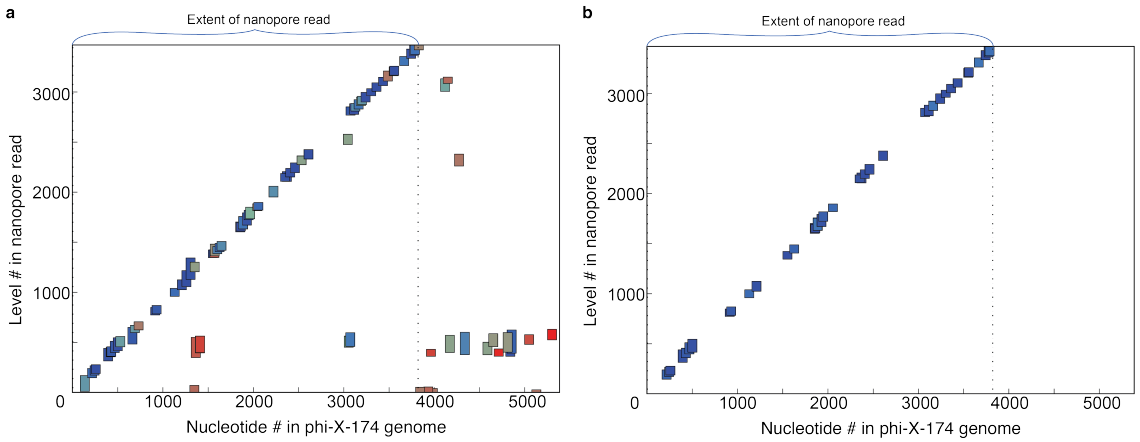

Supplementary figure 12: Alignment-scaffolded assembly of 87 short DNA sequences. Each short DNA sequence is indicated by a box, whose horizontal width indicates the location of the Illumina read within the phi X 174 genome and whose vertical height indicates the span of the Illumina read alignment to a 3466 level nanopore read (spanning 3819 bp in the phi X 174 genome). **a**) Location of all 87 reads that produced alignments to the nanopore read. Color indicates the alignment quality: blue is high-quality and red is low-quality. Overlapping rectangles represent contigs. **b**) After applying a cutoff filter on nanopore alignment quality and the length of the alignment to the nanopore read (keeping only alignments spanning less than 130 levels) we see that all erroneous alignments are filtered out (plus 23 low scoring but correct alignments). Of the 74 Illumina reads which should have aligned to our nanopore read, we are left with 38 (51%) Illumina reads properly localized within the phi X 174 genome with high confidence.

Viral alignment and identification:

Viral identification was performed by aligning arbitrary 250 level subsets of nanopore reads of phi X 174 DNA to a viral database consisting of 5287 viruses (including phi X 174) totaling 156 megabases. To increase the alignment speed, first an 80-level subset of the nanopore read was aligned to every viral genome in the database. This initial alignment was used to generate a list of likely candidate alignments. Alignment confidences for each 80-level alignment to each virus were tallied and compared. Viruses with log confidences better than the mean log confidence score by 3 standard deviations were passed on to the next round; all others were discarded. In the next alignment round, 150 levels of the nanopore read were aligned to the remaining viruses followed by another round of database reduction. Finally all 250 levels were aligned to the remaining viruses. For each event tested, the 250-level alignment correctly identified the DNA as belonging to phi X 174 with at least 99.9996% confidence (in all instances, the 80 or 150-level alignment also suggested phi X 174 as the most likely although with reduced confidence).

Performing a final alignment of the entire >1000-level nanopore reads to the phi X 174 genome can confirm the conclusion to almost arbitrarily high confidence (less than 1 in 10^{70} chance of mis-identification).

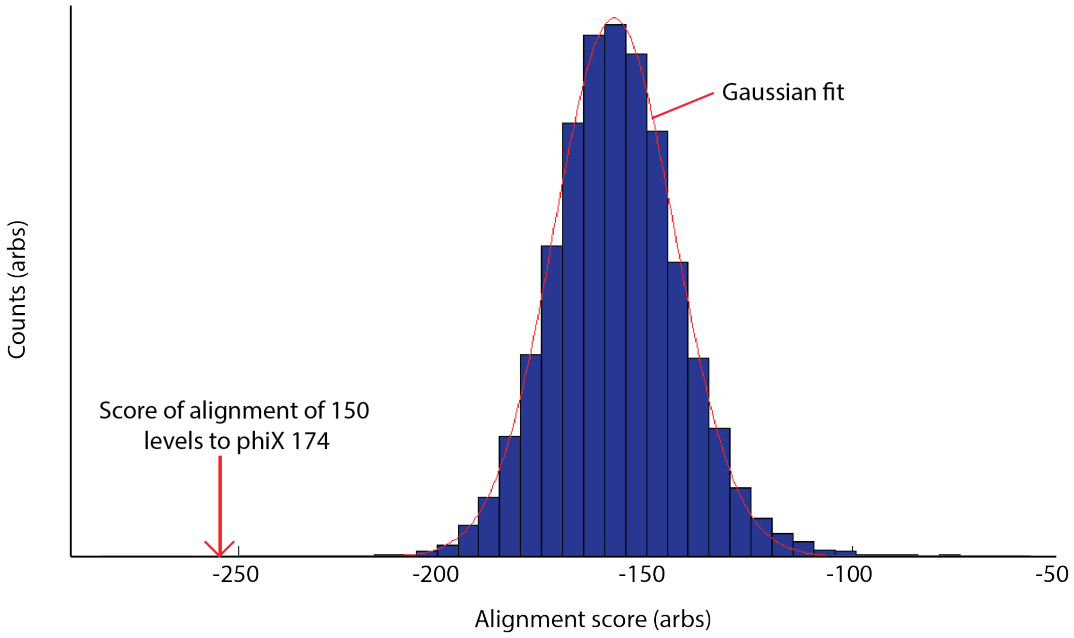

Supplementary figure 13: Distribution of alignment scores for a 150-level segment from a long nanopore read to a viral genome database. The distribution of scores is Gaussian. Here the 150-level alignment to phi X 174 differs from random alignments by ~6.5 standard deviations, identifying the strand with 99.9999997% confidence.

SNP calling workflow schematic

1) We began with measured reference consensus made from several phi X 174 reads

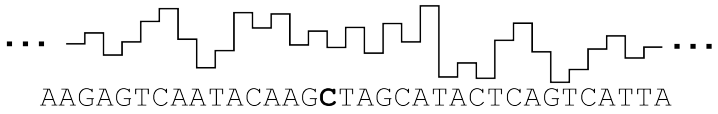

2) We inserted fake SNP's by altering sections of the reference consensus with quadromer map values for the SNP. In this illustration, a **C** is replaced with a **T**.

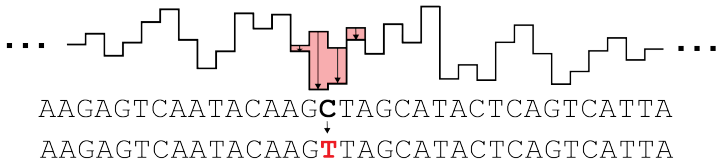

3) We then aligned several nanopore reads to the modified consensus. In general reads aligned quite well to the consensus, alignment errors may occur near inserted SNP's. We used alignments to identify the region of the nanopore reads that will be scrutinized for making the SNP call.

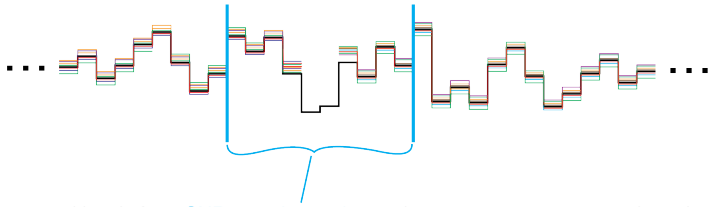

4) We extracted measured levels from SNP-covering region and generate a consensus using a local consensus generating algorithm which aligns multiple sequences to one another and generates a consensus.

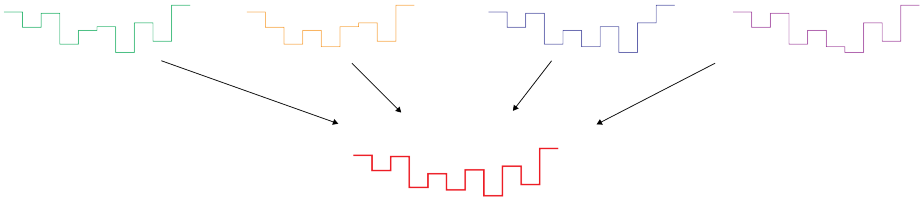

5) Finally we aligned the consensus to the two different SNP possibilities and made a call. Alignments to incorrect sequence resulted in errors (skips, backsteps, holds, bad levels) which decreased the quality of the alignment score. The DNA sequence that matched best with the consensus was called as the measured nucleotide. Including prior probabilities for allele frequency can be used to increase calling accuracy.

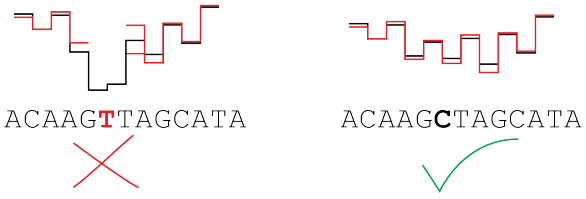

Supplementary figure 14: Schematic outline of SNP detection methods. We inserted "mock SNPs" into a reference consensus by inserting quadromer map values corresponding to the inserted SNP. Transversions and transitions were inserted into the genome in the following ratio (70% C<–>T/G<–>A, 15% C<–>A/G<–>T, 9% G<–>C, and 5% A<–>T) corresponding to how often they occur within the human genome (3). We then performed alignments of nanopore reads to the reference consensus as if we were comparing new nanopore reads to a previously measured consensus. We used these alignments to extract current levels from events that had reads of the SNP region in question. We then generate a consensus using these nanopore measurements. The sequence that aligns best with the consensus is selected as the measured allele. See **Sup. Fig. 16** for detection efficiencies.

SNP detection efficiencies and resequencing confusion matrix

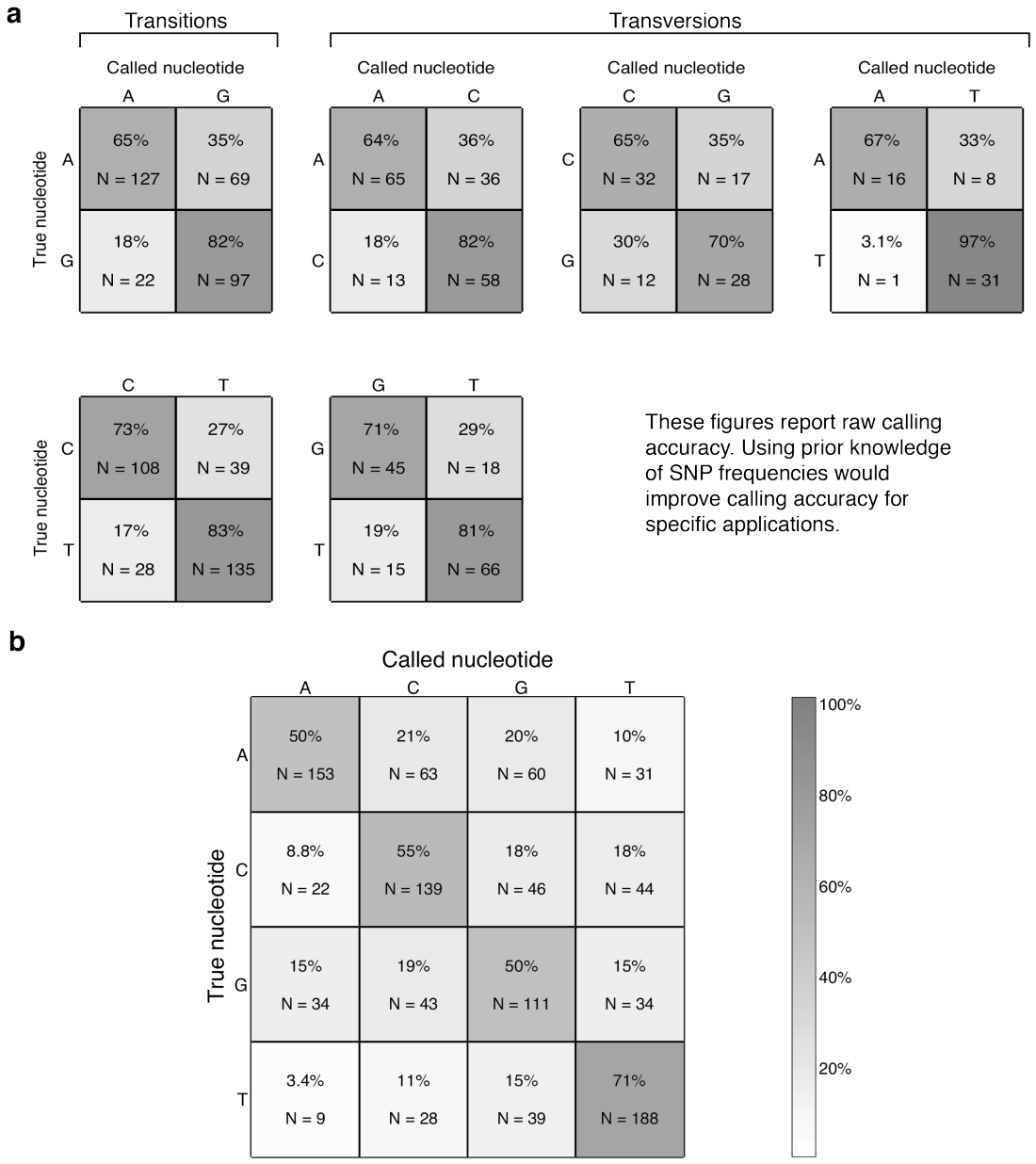

Supplementary figure 15: Confusion matricies for SNPs and reference sequencing. a) Detection efficiencies for each possible SNP in each box. The actual DNA nucleotide is displayed along the left of each box while the nanopore call is displayed along the top of each box. The contrast within the box indicates our ability to distinguish between the two nucleotides in various sequence contexts. **b**) shows detection efficiency for reference sequencing where instead of comparing only two nucleotides (as one does when interrogating most SNPs), we select the nucleotide that matches the data best out of all four nucleotides. Combining reads of both sense and anti-sense strands can increase calling accuracy.

Supplementary Table 1.1: DNA strands used in this study:

Construct	Sequence	# of Pores	# of Events
deBruijn Section 1	5' PAAAAAAACCTTCCXTTTTCCCGTCCGCCTCGTTCGGCGCCTGTCTGCTTTTCGTGTGCCGGTCGGCTAAGCATTCTCATGCAGGTCGTAGCC 3'	4	7
Nucleotide number	0 5 10 15 20 25 30 35 40 45 50 55 60 65 70 75 80 85 90		
DNA purpose	(--Calibration--)(----------Sequence----------)(--Blocker--)(--Primer--)		
deBruijn Section 1 Blocker	5' TTAGCCGACCGGCACACGCAAACAAGCAGACAXXXXXXZ 3'		
Nucleotide number	0 5 10 15 20 25 30 35 40		
deBruijn Section 2	5' PAAAAAAACCTTCCXTGTTTGCGTGTCCCGGTCGGCTGGTTGGCGGGTGGGCCCATCAAAACACTCATAAGCATTCTCATGCAGGTCGTAGCC 3'	7	14
Nucleotide number	0 5 10 15 20 25 30 35 40 45 50 55 60 65 70 75 80 85 90		
DNA purpose	(--Calibration--)(----------Sequence----------)(--Blocker--)(--Primer--)		
deBruijn Section 2 Blocker	5' TTATGAGTGTTTTCATGGGCCCACCCCCCCAAXXXXXXZ 3'		
Nucleotide number	0 5 10 15 20 25 30 35 40		
deBruijn Section 3	5' PAAAAAAACCTTCCXGTGGGCCCATCCAGCCACTCATTCAGTCACGCATGCAGGCACACCTATCTAGCTAAGCATTCTCATGCAGGTCGTAGCC 3'	5	12
Nucleotide number	0 5 10 15 20 25 30 35 40 45 50 55 60 65 70 75 80 85 90		
DNA purpose	(--Calibration--)(----------Sequence----------)(--Blocker--)(--Primer--)		
deBruijn Section 3 Blocker	5' TTAGCTAGATAGGTGTGCCTGCATGCCGTGACTXXXXXXZ 3'		
Nucleotide number	0 5 10 15 20 25 30 35 40		
deBruijn Section 4	5' PAAAAAAACCTTCCXATGCAGGCACACCTATCTAGCTACTTATTTAGTTACGTATGTAGGTACATATACAAGCATTCTCATGCAGGTCGTAGCC 3'	5	11
Nucleotide number	0 5 10 15 20 25 30 35 40 45 50 55 60 65 70 75 80 85 90		
DNA purpose	(--Calibration--)(----------Sequence----------)(--Blocker--)(--Primer--)		
deBruijn Section 4 Blocker	5' TTGTATATGTACCTACATACGTAACTAAATAAXXXXXXXZ 3'		
Nucleotide number	0 5 10 15 20 25 30 35 40		
Legend			
X = abasic site			
Z = 3-carbon spacer			
P = phosphate group			

Supplementary Table 1.2: DNA strands used in this study:

Construct	Sequence	# of Pores	# of Events
deBruijn Section 5	5' PAAAAAAAACCTTCCXTTACGTATGTAGGTACATATACCGATCGAGCCGACTGATTTGAGTGACGGATGGAGAAGCATTTCTCATGCAGGTCGTAGCC 3'	6	12
Nucleotide number	0 5 10 15 20 25 30 35 40 45 50 55 60 65 70 75 80 85 90		
DNA purpose	(--Calibration--)(----------Sequence----------)(--Blocker--)(--Primer--)		
deBruijn Section 5 Blocker	5' TTTCTCCATCCGTCACTCAATCAGTCGCTCGATXXXXXXXZ 3'		
Nucleotide number	0 5 10 15 20 25 30 35 40		
deBruijn Section 6	5' PAAAAAAAACCTTCCXACTGATTGAGTGACGGATGGAGGCACAGATAGAGACCAATCAAGCAACTAATAAAAGCATTCTCATGCAGGTCGTAGCC 3'	3	15
Nucleotide number	0 5 10 15 20 25 30 35 40 45 50 55 60 65 70 75 80 85 90		
DNA purpose	(--Calibration--)(----------Sequence----------)(--Blocker--)(--Primer--)		
deBruijn Section 6 Blocker	5' TTTTATTAGTTGCTTGATTXXXXXXZ 3'		
Nucleotide number	0 5 10 15 20 25		
deBruijn Section 7	5' PAAAAAAAACCTTCCXAGACCAATCAAGCAACTAATTAAGTAACGAATGAAGGAACAAATAAAGAAAACCAAGCATTCTCATGCAGGTCGTAGCC 3'	8	11
Nucleotide number	0 5 10 15 20 25 30 35 40 45 50 55 60 65 70 75 80 85 90		
DNA purpose	(--Calibration--)(----------Sequence----------)(--Blocker--)(--Primer--)		
deBruijn Section 7 Blocker	5' TTGGTTTTCTTTATTTGTTCCTTCATTCGTTTACTTTAXXXXXXXZ 3'		
Nucleotide number	0 5 10 15 20 25 30 35 40 45		
deBruijn Section 8	5' PAAAAAAAACCTTCCXGAAGGAACAAATAAAGAAAACCCCTCTCCTTCTTTTCCCGTCCGCTCGTTCGCGAAGCATTCTCATGCAGGTCGTAGCC 3'	1	17
Nucleotide number	0 5 10 15 20 25 30 35 40 45 50 55 60 65 70 75 80 85 90		
DNA purpose	(--Calibration--)(----------Sequence----------)(--Blocker--)(--Primer--)		
deBruijn Section 8 Blocker	5' TTCGCGAACGAGCGGACGGXXXXXXXZ 3'		
Nucleotide number	0 5 10 15 20 25		
deBruijn Primer	5' GCGTACGCCTACGGTTTTCCGTAGGCGTACGCGGCTACGACCTGCATGAGAATGC 3'		
Nucleotide number	0 5 10 15 20 25 30 35 40 45 50 55		
Phi X Adaptor	5' PZAAAAAAAACCTTCCZCCTTCCCATCATCAGATCTCACGCGG 3'		
Nucleotide number	0 5 10 15 20 25 30 35 40 45		
Phi X Hairpin (1)	5' PCGCCTACGGTTTTTCCGTAGGCGTACGCUTACTTGTACTTGGCGG 3'		
Nucleotide number	0 5 10 15 20 25 30 35 40 45		
Phi X Hairpin (2)	5' CCGCCAAGTACAAGTAAGCGTA 3'		
Nucleotide number	0 5 10 15 20 25		
Legend			
X = abasic site			
Z = 3-carbon spacer			
P = phosphate group			

Supplementary Table 2.1: Table of quadromer map values beginning with A.

Quadromer	de Bruijn Value (pA)	Revised Value (pA)	Error on Revised Value (pA)	Number of Phi X 174 Measurements
AAAA	45.8	46.2	1.4	65
AAAC	42.1	42.1	1.3	45
AAAG	47.5	48.5	1.4	34
AAAT	46.4	47.3	1.7	52
AACA	46.4	46.8	1.1	27
AACC	39.3	38.7	0.8	45
AACG	41.6	41.4	0.9	42
AACT	39.7	39.7	1.0	57
AAGA	47.5	48.0	1.2	42
AAGC	41.5	41.4	1.2	25
AAGG	45.2	45.2	1.2	25
AAGT	44.4	43.0	1.6	36
AATA	40.2	40.1	0.9	44
AATC	35.2	34.1	1.5	34
AATG	39.4	38.7	1.4	29
AATT	36.7	35.4	1.8	54
ACAA	46.4	46.4	1.3	34
ACAC	43.4	43.1	0.8	15
ACAG	44.7	44.8	1.0	23
ACAT	45.2	45.9	1.4	16
ACCA	42.7	43.0	1.0	50
ACCC	40.7	41.0	0.9	14
ACCG	46.3	45.4	0.7	40
ACCT	41.5	41.5	1.0	34
ACGA	46.6	46.5	0.6	48
ACGC	39.7	39.9	1.3	31
ACGG	44.5	44.4	0.8	26
ACGT	42.3	41.6	1.5	30
ACTA	41.9	42.1	1.3	43
ACTC	37.4	37.1	0.8	41
ACTG	40.1	39.3	1.4	42
ACTT	36.1	35.3	1.7	48
AGAA	56.3	55.1	1.6	43
AGAC	45.0	44.6	1.2	36
AGAG	54.1	53.0	1.3	29
AGAT	47.7	49.3	2.2	19
AGCA	49.1	48.9	1.5	26
AGCC	41.8	41.0	1.4	26
AGCG	51.7	50.4	1.4	26
AGCT	44.0	43.1	1.1	20
AGGA	47.9	47.7	1.1	26
AGGC	38.3	38.8	1.4	13
AGGG	41.8	40.6	2.0	11
AGGT	37.4	37.6	1.3	39
AGTA	31.5	31.4	1.4	53
AGTC	24.3	23.3	1.8	50
AGTG	34.6	33.8	1.9	30
AGTT	27.3	25.2	1.4	60
ATAA	44.6	44.5	0.9	37
ATAC	42.5	41.5	1.0	33
ATAG	42.0	42.8	0.8	41
ATAT	42.8	42.3	0.9	16
ATCA	37.2	37.5	1.1	20
ATCC	35.3	34.4	1.1	17
ATCG	39.8	39.3	1.0	28
ATCT	37.4	37.3	0.9	26
ATGA	36.4	36.4	1.1	25
ATGC	30.7	31.0	1.0	25
ATGG	36.0	35.6	0.8	29
ATGT	33.0	31.7	1.4	14
ATTA	31.6	31.1	0.9	46
ATTC	26.4	25.0	1.0	33
ATTG	31.4	30.6	1.2	39

Supplementary Table 2.2: Table of quadromer map values beginning with C.

Quadromer	de Bruijn Value (pA)	Revised Value (pA)	Error on Revised Value (pA)	Number of Phi X 174 Measurements
CAAA	46.4	46.1	1.1	36
CAAC	43.5	43.1	1.4	41
CAAG	47.5	46.7	1.3	30
CAAT	43.2	43.3	1.2	31
CACA	47.1	46.9	1.3	15
CACC	40.6	40.3	1.1	20
CACG	39.7	39.4	1.0	18
CACT	41.1	40.8	0.8	20
CAGA	47.7	47.8	1.5	22
CAGC	37.0	37.1	1.2	31
CAGG	42.9	43.0	0.8	18
CAGT	37.4	39.1	1.7	51
CATA	42.8	42.6	1.0	31
CATC	35.3	35.1	1.3	25
CATG	38.9	39.4	1.0	18
CATT	31.4	33.1	2.0	34
CCAA	45.3	45.1	1.0	34
CCAC	42.7	42.3	0.7	15
CCAG	43.7	44.0	1.1	29
CCAT	43.3	44.5	1.3	36
CCCA	46.3	45.5	1.1	15
CCCC	42.6	42.4	1.2	10
CCCG	43.0	43.3	1.2	7
CCCT	37.8	38.0	1.4	19
CCGA	46.3	46.2	0.9	28
CCGC	40.7	40.7	1.1	40
CCGG	43.2	44.2	0.8	19
CCGT	38.0	37.9	1.9	33
CCTA	43.9	43.8	0.9	26
CCTC	37.8	37.4	0.9	27
CCTG	34.1	35.2	1.7	18
CCTT	32.8	33.6	1.7	38
CGAA	51.3	50.6	0.9	58
CGAC	42.4	41.8	1.2	44
CGAG	46.4	46.1	0.7	32
CGAT	44.4	44.1	1.1	19
CGCA	47.8	46.4	1.4	45
CGCC	40.2	39.9	1.0	31
CGCG	43.1	43.5	0.9	26
CGCT	40.7	40.9	0.8	30
CGGA	40.7	39.6	1.3	28
CGGC	33.5	33.8	1.0	25
CGGG	36.2	36.7	1.8	9
CGGT	31.6	31.8	2.0	43
CGTA	27.0	26.2	1.5	41
CGTC	16.8	16.6	1.6	49
CGTG	21.8	21.4	1.4	19
CGTT	17.7	17.9	1.3	58
CTAA	47.3	46.5	1.3	48
CTAC	40.4	40.1	0.9	34
CTAG	44.8	44.4	1.8	1
CTAT	37.0	37.5	1.1	40
CTCA	44.1	43.6	0.9	30
CTCC	37.5	37.2	1.0	27
CTCG	35.7	35.7	2.3	32
CTCT	38.6	38.2	0.9	34
CTGA	34.3	34.5	1.1	24
CTGC	27.5	27.9	1.0	38
CTGG	34.1	33.8	1.0	23
CTGT	24.5	26.1	2.1	22
CTTA	31.2	30.3	1.0	36
CTTC	22.1	22.3	0.9	52
CTTG	27.4	27.3	0.8	33
CTTT	24.0	23.6	1.1	66

Supplementary Table 2.3: Table of quadromer map values beginning with G.

Quadromer	de Bruijn Value(pA)	Revised Value(pA)	Error on Revised Value (pA)	Number of Phi X 174 Measurements
GAAA	56.3	54.3	1.3	50
GAAC	44.6	44.1	1.1	44
GAAG	48.7	49.3	1.9	38
GAAT	48.6	50.0	1.6	31
GACA	45.8	45.1	1.2	24
GACC	38.7	38.6	0.9	30
GACG	42.2	42.4	0.9	38
GACT	39.7	40.4	1.5	49
GAGA	47.4	49.1	1.2	23
GAGC	43.3	43.4	1.2	21
GAGG	43.4	43.8	1.3	16
GAGT	45.4	45.2	1.8	49
GATA	41.0	40.5	0.9	16
GATC	33.9	33.9	2.3	6
GATG	39.4	39.2	1.3	18
GATT	35.6	35.1	1.9	24
GCAA	49.1	48.8	0.8	41
GCAC	38.7	39.1	1.5	22
GCAG	48.0	47.8	1.4	35
GCAT	38.9	38.8	1.3	21
GCCA	44.4	44.7	0.7	22
GCCC	41.5	41.2	1.4	8
GCCG	43.2	43.9	1.0	41
GCCT	41.3	41.5	0.8	21
GCGA	47.2	47.3	0.6	23
GCGC	38.6	38.8	1.2	22
GCGG	45.6	45.5	1.0	29
GCGT	37.2	38.1	1.9	35
GCTA	36.8	37.1	1.3	21
GCTC	33.7	34.2	1.4	20
GCTG	36.0	36.6	1.3	26
GCTT	31.6	32.9	1.6	33
GGAA	51.8	52.2	1.6	32
GGAC	41.8	41.5	1.6	26
GGAG	46.7	47.4	1.2	27
GGAT	44.1	44.3	1.5	11
GGCA	43.7	43.6	1.7	18
GGCC	40.0	39.3	1.6	8
GGCG	42.3	42.2	1.5	22
GGCT	37.9	38.3	1.8	17
GGGA	41.8	41.3	1.8	14
GGGC	31.3	31.7	1.5	6
GGGG	30.2	31.1	4.6	7
GGGT	30.7	30.9	2.4	15
GGTA	28.0	27.8	1.8	44
GGTC	17.8	17.1	1.8	40
GGTG	25.5	24.7	1.3	24
GGTT	20.3	19.9	1.6	54
GTAA	40.3	39.3	1.7	47
GTAC	38.5	37.5	1.9	31
GTAG	38.0	38.3	1.4	42
GTAT	37.4	37.2	1.7	44
GTCA	35.7	35.9	2.4	34
GTCC	27.4	26.3	2.1	31
GTCG	30.6	29.2	2.0	58
GTCT	28.5	27.1	1.7	46
GTGA	33.5	31.7	2.0	23
GTGC	24.4	24.9	1.8	24
GTGG	22.9	24.0	1.9	25
GTGT	26.9	26.9	1.4	21
GTTA	29.5	27.8	1.9	49
GTTC	21.2	20.1	1.8	47
GTTG	27.5	25.9	1.6	45
GTTT	22.2	21.4	1.2	65

Supplementary Table 2.4: Table of quadromer map values beginning with T.

Quadromer	de Bruijn Value (pA)	Revised Value (pA)	Error on Revised Value (pA)	Number of Phi X 174 Measurements
TAAA	44.6	44.7	1.2	56
TAAC	42.5	42.4	0.9	39
TAAG	47.6	47.5	1.0	28
TAAT	50.5	48.7	1.2	48
TACA	44.4	44.3	1.4	24
TACC	42.5	42.0	1.2	41
TACG	42.3	42.5	1.0	37
TACT	43.2	43.2	0.8	47
TAGA	45.8	45.3	1.1	32
TAGC	41.3	41.4	1.0	20
TAGG	44.0	44.8	0.7	29
TAGT	41.8	42.9	1.3	56
TATA	40.7	40.9	0.9	34
TATC	36.1	35.5	1.0	26
TATG	37.9	38.3	1.2	31
TATT	35.0	36.0	1.1	61
TCAA	43.7	43.0	1.1	30
TCAC	39.7	39.0	1.1	23
TCAG	46.3	44.8	1.3	35
TCAT	48.1	46.5	1.4	36
TCCA	43.7	42.6	1.3	28
TCCC	38.6	39.5	1.1	18
TCCG	39.3	40.8	1.6	32
TCCT	41.2	40.7	1.0	35
TCGA	46.4	45.2	2.0	42
TCGC	40.4	40.0	1.2	37
TCGG	40.0	41.0	1.5	30
TCGT	37.9	38.9	1.4	71
TCTA	42.1	41.3	1.2	33
TCTC	34.6	34.8	0.9	34
TCTG	32.8	33.1	1.3	23
TCTT	32.4	33.1	1.4	68
TGAA	45.6	46.0	2.1	31
TGAC	38.5	38.6	1.1	32
TGAG	42.4	43.1	1.2	24
TGAT	43.3	43.3	1.3	16
TGCA	42.8	42.4	1.7	28
TGCC	35.4	35.9	1.6	27
TGCG	40.6	40.4	1.7	43
TGCT	37.3	37.9	1.3	34
TGGA	38.7	38.6	1.3	27
TGGC	32.1	32.5	1.1	21
TGGG	33.7	33.8	1.0	14
TGGT	27.1	28.0	1.7	64
TGTA	27.1	27.0	1.6	27
TGTC	17.6	17.1	1.4	32
TGTG	21.7	21.7	1.1	19
TGTT	18.8	18.6	1.0	35
TTAA	40.1	40.4	1.6	39
TTAC	35.6	35.6	1.2	53
TTAG	41.8	41.2	1.3	53
TTAT	40.6	39.8	1.1	51
TTCA	36.0	34.8	1.6	40
TTCC	28.7	28.6	1.3	39
TTCG	33.2	32.5	1.6	62
TTCT	32.4	31.6	1.6	46
TTGA	33.1	32.8	1.2	30
TTGC	27.3	27.6	1.0	45
TTGG	32.1	32.0	1.0	46
TTGT	28.8	28.8	0.8	55
TTTA	29.2	28.3	1.3	67
TTTC	22.2	21.8	1.1	58
TTTG	25.9	26.2	0.9	63
TTTT	22.2	22.8	0.9	89

References:

20. Needleman SB & Wunsch CD (1970) A General Method Applicable to Search for Similarities in Amino Acid Sequence of 2 Proteins. *Journal of Molecular Biology* 48(3):443-453.
21. Durbin R, Eddy S, Krogh A, & Mitchison G (2006) *Biological sequence analysis* pp 92-96.
33. Dawson E*, et al.* (2001) A SNP resource for human chromosome 22: extracting dense clusters of SNPs from the genomic sequence. *Genome Res* 11(1):170-178.